

# SatHealth: A Multimodal Public Health Dataset with Satellite-based Environmental Factors

Yuanlong Wang  
wang.16050@osu.edu  
The Ohio State University  
Columbus, Ohio, USA

Changchang Yin  
yin.731@osu.edu  
The Ohio State University  
Columbus, Ohio, USA

Pengqi Wang  
wang.19883@osu.edu  
The Ohio State University  
Columbus, Ohio, USA

Ping Zhang\*  
zhang.10631@osu.edu  
The Ohio State University  
Columbus, Ohio, USA

## Abstract

Living environments play a vital role in the prevalence and progression of diseases, and understanding their impact on patient's health status becomes increasingly crucial for developing AI models. However, due to the lack of long-term and fine-grained spatial and temporal data in public and population health studies, most existing studies fail to incorporate environmental data, limiting the models' performance and real-world application. To address this shortage, we developed SatHealth, a novel dataset combining multimodal spatiotemporal data, including environmental data, satellite images, all-disease prevalences estimated from medical claims, and social determinants of health (SDoH) indicators. We conducted experiments under two use cases with SatHealth: regional public health modeling and personal disease risk prediction. Experimental results show that living environmental information can significantly improve AI models' performance and temporal-spatial generalizability on various tasks. Finally, we deploy a web-based application<sup>1</sup> to provide an exploration tool for SatHealth and one-click access to both our data and regional environmental embedding to facilitate plug-and-play utilization. SatHealth is now published with data in Ohio, and we will keep updating SatHealth to cover the other parts of the US. With the web application and published code pipeline<sup>2</sup>, our work provides valuable angles and resources to include environmental data in healthcare research and establishes a foundational framework for future research in environmental health informatics.

## CCS Concepts

• **Applied computing** → *Health informatics*; • **Social and professional topics** → *Medical records*; • **Computing methodologies** → *Learning latent representations*.

\*Corresponding Author

<sup>1</sup> <https://aimed-sathealth.net>

<sup>2</sup> <https://github.com/Wang-Yuanlong/SatHealth>



This work is licensed under a Creative Commons Attribution-ShareAlike 4.0 International License.

*KDD '25, Toronto, ON, Canada*

© 2025 Copyright held by the owner/author(s).

ACM ISBN 979-8-4007-1454-2/2025/08

<https://doi.org/10.1145/3711896.3737440>

## Keywords

Satellite Images, Environmental Health Informatics, Social Determinants of Health, Medical Records, AI in Public Health

## ACM Reference Format:

Yuanlong Wang, Pengqi Wang, Changchang Yin, and Ping Zhang. 2025. SatHealth: A Multimodal Public Health Dataset with Satellite-based Environmental Factors. In *Proceedings of the 31st ACM SIGKDD Conference on Knowledge Discovery and Data Mining V.2 (KDD '25), August 3–7, 2025, Toronto, ON, Canada*. ACM, New York, NY, USA, 18 pages. <https://doi.org/10.1145/3711896.3737440>

## 1 Introduction

The living environment (e.g., climate, green spaces, air quality, and socioeconomic factors) considerably impacts people's physical [20, 25] and mental [71] health, and understanding such impact is an emerging topic [18, 33, 39]. Considerable efforts have been made to explore how these factors are associated with human health [37, 62, 67]. However, due to the complexity of aligning multi-source geospatial data with medical data, there are still limited handy medical datasets equipped with high spatiotemporal resolution, long-term coverage, and comprehensive environmental data. Therefore, existing studies either focus on specific diseases and environmental factors [14, 41] or take solely patients' medical record histories without consideration of environmental factors [13, 73, 78, 79]. As a result, these models might be limited in their accuracy, comprehensiveness, and spatiotemporal robustness. Moreover, the benefit of information from the living environment in healthcare AI remains unexplored.

To fill the shortage, we propose a pipeline and develop SatHealth, a compound dataset featuring satellite-based environmental data, satellite imagery, prevalence of all diseases estimated from medical claims, and Social Determinants of Health (SDoH) indices. To the best of our knowledge, SatHealth is the first dataset in the US that combines regional environmental characteristics with a healthcare database. We requested over 400k aerial view satellite images from Google Maps [28], each image covers about a 500m wide square area. Furthermore, we use medical claims from the MarketScan [45] database to estimate the regional prevalence for all diseases. As for SDoH, we use the Social Deprivation Index (SDI) [34], which is a comprehensive score calculated from US census data from the American Community Survey (ACS) [9]. Moreover, we designed

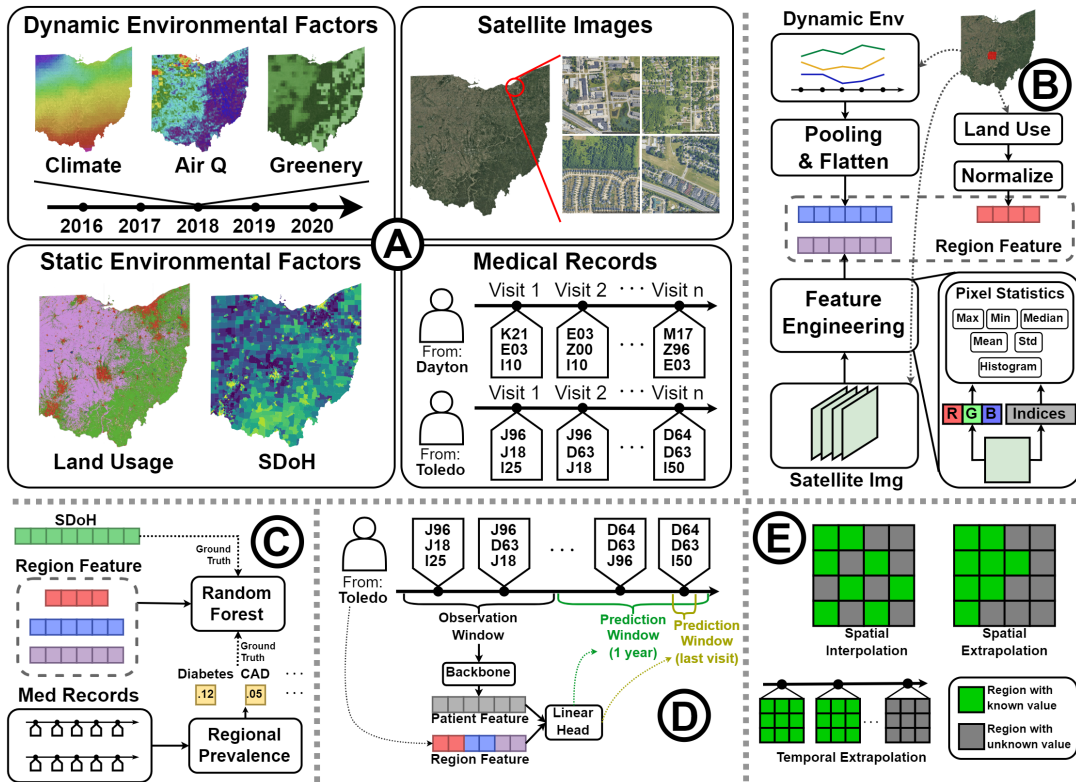


**Figure 1: Overview of SatHealth and Experimental framework. (A) The components of SatHealth. (B) The regional embedding pipeline. We use all dynamic factors, satellite images, and land usage as the multimodal environmental features of a region. (C) We use the regional embedding to predict the prevalence of all kinds of diseases and SDoH within that region. (D) We combine patient representation with the regional embedding of patient residence to predict patient disease risk. (E) We test model robustness on three generalization scenarios.**

a multimodal fusion framework to seamlessly integrate heterogeneous multimodal environmental data sources and provide user-friendly regional environment embeddings, facilitating downstream analyses and follow-up studies.

We first validated and quantified the environmental-disease relationship by statistical testing, reflecting the disparity in urban-rural health status. After that, we use the dataset on two clinical tasks: regional public health modeling (e.g., to predict regional SDI scores and disease prevalence based on environmental data) and personalized disease risk prediction (e.g., to enhance personal disease risk prediction with environmental data). The experimental results show that living environmental information can significantly improve AI models’ performance and spatiotemporal generalizability. Finally, we deployed a web-based application<sup>1</sup> where users could explore and access SatHealth data with regional embedding vectors. Our regional embeddings can be plugged into any clinical AI with geospatial information, which paves the way for integrating environmental factors into clinical AI development.

We started SatHealth development from Ohio as a concomitant of the Ohio O-SUDDen program [23]. However, all satellite data we use have global coverage, and MarketScan patient-level medical claims have US coverage. Therefore, our framework’s environmental factor processing pipeline can be easily adapted to other areas. We also provide our code on GitHub<sup>2</sup> so that users can create data

and embeddings for different areas of interest. We will also gradually update SatHealth to cover the US in the future.

In summary, we summarize our contributions as follows:

- We construct SatHealth, the first publicly available dataset in the US consisting of environmental data, satellite imagery, regional SDoH, and all-disease prevalence for comprehensive environment-health analysis.
- We design an embedding pipeline to construct regional environment embeddings by fusing multimodal data from SatHealth.
- We show two use cases of SatHealth. The experimental results exhibit the benefit of environmental information in model accuracy and temporal-spatial generalizability.
- We deployed a web-based application to showcase and provide access to SatHealth and our embeddings. We also publish our code for data collection in other areas of interest.

**Code and Docs:** <https://github.com/Wang-Yuanlong/SatHealth>

**Web app and Dataset download:** <https://aimed-sathealth.net>

**License:** The dataset is released under the CC BY-SA 4.0 license.

## 2 Related Works

### 2.1 Environment-health Datasets

Environmental factors, such as built environment, air quality, and green space, are reported to be correlated with many diseases, such

**Table 1: A comparison of SatHealth to related datasets combining environmental and health data**

Dataset	Location	Target	Target data source	Imagery	Year span	Public
Barboza et al.	31 European countries	Mortality	Eurostat	✗	2015	✗
Temenos et al.	8 European cities	COVID-19	OWD	✗	2020-2021	✗
SatelliteBench	81 municipalities in Colombia	Dengue outbreak, Poverty, Access to school	SIVIGILA, Census	Sentinel-2	2016-2018	✓
SustainBench	Global	BMI, child mortality, water quality, sanitation	Surveys	LandSat, Street view	1996-2019	✓
MedSat	England	Medical prescription of 7 conditions	NHS	Sentinel-2	2019-2020	✓
<b>SatHealth</b>	Ohio, US	SDoH, All ICD code prevalence	SDI, MarketScan	Google Maps	2016-2022	✓

OWD: Our World in Data platform; NHS: National Health Services; SIVIGILA: Colombian Public Health Surveillance System

as heart diseases [14, 15], metabolic syndrome [38], and stroke [4]. Researchers construct datasets with earth observation (EO) and remote sensing data with various health outcomes to learn their health impacts. For example, Barboza et al. [7] and Temenos et al. [64] collected regional greenery indices like normalized difference vegetation index (NDVI) and percentage of green area (%GA), and studied their relationship with natural-cause mortality and COVID-19 cases. However, the greenery indices provide a limited expression of the living environment. Therefore, some datasets include satellite images to capture a more comprehensive neighborhood view. SatelliteBench [48] examines the dengue outbreak in 81 Colombian municipalities, collecting Sentinel-2 satellite images, climate, socioeconomic factors, and dengue cases to predict poverty, school access, and dengue outbreaks. Moreover, SustainBench [75] benchmarks prediction tasks of 4 public health indicators from surveys with satellite images and street view panorama. However, These datasets rely on public health surveys, which limit their target scope. Recently, MedSat [58] was developed in England by integrating sociodemographic features, satellite imagery, environmental variables, and prescription data. However, it is constrained by indirect prevalence estimation, leading to higher errors and limited disease scope. Finally, all these datasets suffered from a limited scope of target disease and none or moderate-resolution satellite images. Inspired by all these works, we developed SatHealth by combining SDoH, environmental variables, satellite images, and the MarketScan medical claim database. High-resolution satellite images from Google Maps provide a clear view of ground-level environments, while MarketScan provides prevalence estimates for thousands of diseases. Hence, SatHealth enables comprehensive environment-health analyses.

## 2.2 Health-related Target Modeling

**Environment-health relationship modeling.** Numerous studies have been conducted to explore the impact of the environment on human health. The fundamental methods are community surveys and statistical tests. Wafula et al. [67] used surveys and mediation analysis to explore socioeconomic disparities in malaria prevalence in Malawi. Similarly, Keenan et al. [37] analyzed multidrug-resistant urinary tract infections (MDR UTIs) in East Africa using questionnaires and Bayesian profile regression to identify clusters of social and environmental determinants. By incorporating image modalities, Zhang et al. [80] explored the protective effects of shaded environments against adolescent myopia using commercial satellite maps and Spearman’s correlation analysis.

Machine learning methods are also widely adopted. For example, Araújo et al. [3] employed Sentinel-1 and Sentinel-2 data to investigate the relationship between green spaces and mental health, using

spatial autocorrelation metrics like Moran’s I and regression models to quantify the impact of environmental features. Yin et al. [77] and Nazia et al. [50] applied Bayesian hierarchical models to study the dynamics of COVID-19 spread, incorporating environmental, social, and health data. Luo et al. [41] used mixed-effects models to analyze the association between air pollution and hypertension, revealing disparities in cardiovascular health risks. At the same time, Gibb et al. [26] employed Bayesian spatiotemporal modeling to investigate dengue emergence linked to climate change and urban infrastructure. Most recently, Chen et al. [14] investigated the correlation between built environment from street view and coronary artery disease prevalence using deep learning-based features. They also explored the correlation between satellite imagery and cardiometabolic diseases [15]. However, these works focus on some specific diseases without a broader understanding of the impact of the environment on diverse diseases.

**Personalized disease risk prediction.** Predictive risk modeling predicts patients’ future disease status based on their historical medical records. Electronic health records (EHR) are generally used to provide patient medical history. As EHR data can be modeled naturally as sequential data, several deep-learning methods have been employed in previous studies for risk prediction. RETAIN [17] uses reverse time attention to capture health status from the most recent patient visits. Dipole [43] uses a bidirectional recurrent neural network to capture more complex time dependencies in EHR. In recent years, there are also transformer-based models [42, 74] and knowledge-enriched models [16, 44]. However, these models focus solely on personal patient status without utilizing information from patients’ living environments. We fill this gap by plugging our environmental embedding into patient representation according to their residence.

## 3 SatHealth Dataset

In this section, we introduce the SatHealth dataset by four components: SDoH, Environmental data, satellite imagery, and disease prevalence, as shown in Table 2. Besides data collection, we will introduce our embedding pipeline for environmental data and satellite images. We embed environmental data and satellite images across multiple geographic-level regions, including counties, ZIP Code Tabulation Areas (ZCTAs), census tracts, and Core Based Statistical Areas (CBSAs), ensuring comprehensive spatial granularity.

### 3.1 Social Determinants of Health

Social determinants of health (SDoH) refer to the environmental conditions in which people live, influencing a wide range of health

**Table 2: The number of variables in each category**

	Modality	Category	Statistics
SDoH	Tabular	SDI	8 Variables
Environmental	Tabular	Land Cover	9 Variables
	Time Series (Monthly)	Climate	28 Variables, 7 years
		Air Quality	4 Variables, 7 years
		Greenery	4 Variables, 7 years
Satellite Imagery	Image	-	432918 Images
			3 Channels (RGB)
			9 Calculated Indices
Medical Records	Time Series (Yearly)	ICD code	1377 unique codes
		Prevalence	7 years coverage
			2141777 patients

outcomes and quality of life [53]. These include various socioeconomic factors, such as poverty, access to education, healthcare availability, the built environment, and community context.

**Data Collection.** This work incorporates the Social Deprivation Index (SDI) [34] as the regional socioeconomic indicator. The SDI<sup>3</sup> is a centile score comprised of seven demographic components derived from the American Community Survey (ACS): (1) the percentage of the population living below 100% of the Federal Poverty Level (FPL); (2) the percentage of individuals aged 25 years or older with less than 12 years of education; (3) the percentage of non-employed individuals aged 16–64; (4) the percentage of single-parent families with dependents under 18; (5) the percentage of households without access to a vehicle; (6) the percentage of households residing in renter-occupied units; and (7) the percentage of households living in crowded conditions.

### 3.2 Environmental Data

Environmental data contains four categories: climate, air quality, greenery, and land cover. We collect them from multiple satellite products.

**Data Collection.** We obtained environmental variables for our dataset on Google Earth Engine (GEE) [29] following [58]. Climate variables include temperatures, humidity, solar radiation, snow cover, and wind components from ERA5-ECMWF product [49]. For air quality, we collect nitrogen dioxide (NO<sub>2</sub>) from Sentinel-5P Near Real-Time NO<sub>2</sub> [35], total aerosols and PM<sub>2.5</sub> from Copernicus Atmosphere Monitoring Service (CAMS) [24], and ozone from Total Ozone Mapping Spectrometer (TOMS) and Ozone Monitoring Instrument (OMI) Merged Ozone Data [2]. Greenery variables include Normalized Difference Vegetation Index (NDVI) derived from Sentinel-2 MultiSpectral Instrument (MSI) [1] and high/low vegetation greenery indices from ERA5-ECMWF. Land cover variables are area cover fractions of different land types (e.g., forest, water, urban) sourced from Copernicus Dynamic Land Cover products [60]. We collected all the available data in Ohio from 2016 to 2022.

**Spatiotemporal Alignment.** As shown in Table 8, data from various satellite products have different spatial resolutions and temporal frequencies, so we align them to ensure consistency in both spatial and temporal granularity. Given a specific timestamp and an environment variable, we collect the values in various areas

and obtain a heatmap, with each pixel denoting the value in a square area. We perform spatial reduction to a specific region (e.g., counties) by taking the average of all pixels within the region. After the reduction for every variable, we obtain an environmental vector for each specific region. We further align variables temporally by downsampling all vector series to the same monthly frequency. As land cover fractions are relatively stable, they are averaged across all timestamps to become a static variable.

**Feature Embedding.** After the alignment process, each region has environment data as a multivariate time series. To embed the time series, we average the monthly vectors according to meteorological seasons and concatenate seasonal vectors to create annual regional embedding.

### 3.3 Satellite Images

In addition to environmental variables, satellite images offer additional visual insights into specific regions. By incorporating satellite imagery from Google Maps, we provide an implicit indicator of regional development, environmental characteristics, and land-use patterns.

**Data Collection.** We request aerial images from the Google Static Maps Application Programming Interface (API) [28]. A grid of spatial points with 500-meter spacing is created, and satellite image patches are retrieved at zoom level 17 with grid points. With the point-grid-based construction, we can establish the visual feature of an arbitrary region by aggregating satellite images within that region. This approach ensures complete coverage of Ohio, resulting in 432,918 images with a resolution of 1280×1280 pixels each, corresponding to a square area approximately 500 meters wide.

**Feature Embedding.** We establish visual features by calculating several indices commonly used in remote sensing [10, 22, 30, 81] and computing their pixel-level statistics. For a given RGB aerial image, nine indices are calculated for each pixel based on RGB values, effectively creating new derived channels. These channels form a compound image with 12 channels alongside the original RGB channels. After that, to extract meaningful features from the compound images, we compute pixel-level statistics for each channel, including the mean, standard deviation, median, maximum, minimum, and 20-bin histogram features. This process produces feature vectors of size 300 for each satellite image. Note that images from Google Maps do not have timestamps, so the satellite image feature is static.

### 3.4 Disease Prevalence

We use regional disease prevalence as an indicator of the population health status of an area.

**Data Collection.** We estimate disease prevalence using MarketScan [45], a real-world medical claims database. Specifically, we analyze patient encounters from the MarketScan Commercial Claims and Encounters (CCA) database from 2016 to 2022. Each patient encounter includes a set of International Classification of Diseases (ICD-10) [12] diagnoses codes and the patient’s residency. Patient residency in MarketScan is identified by Metropolitan Statistical Areas (MSAs), a subset of CBSAs. This enables us to estimate

<sup>3</sup><https://www.graham-center.org/maps-data-tools/social-deprivation-index.html>

**Table 3: ICD codes with top Urban-rural relevance by Odds Ratio**

Category	Code	Odds Ratio	95% CI	Description
Urban Prevalent	P00-P96	1.479	(1.418, 1.542)	Certain conditions originating in the perinatal period
	O00-O9A	1.160	(1.131, 1.190)	Pregnancy, childbirth and the puerperium
	R99	0.312	(0.227, 0.427)	Ill-defined and unknown cause of mortality
Rural Prevalent	I00-I99	0.765	(0.756, 0.773)	Diseases of the circulatory system
	I05-I09	0.631	(0.584, 0.681)	Chronic rheumatic heart diseases
	I26-I28	0.735	(0.687, 0.786)	Pulmonary heart disease and diseases of pulmonary circulation
	I60-I69	0.736	(0.701, 0.772)	Cerebrovascular diseases
	I10-I1A	0.743	(0.735, 0.752)	Hypertensive diseases
	E00-E89	0.785	(0.777, 0.793)	Endocrine, nutritional and metabolic diseases
	E40-E46	0.636	(0.583, 0.694)	Malnutrition
	E70-E88	0.737	(0.728, 0.745)	Metabolic disorders
	E65-E68	0.773	(0.761, 0.785)	Overweight, obesity and other hyperalimentation
	E08-E13	0.792	(0.778, 0.806)	Diabetes mellitus

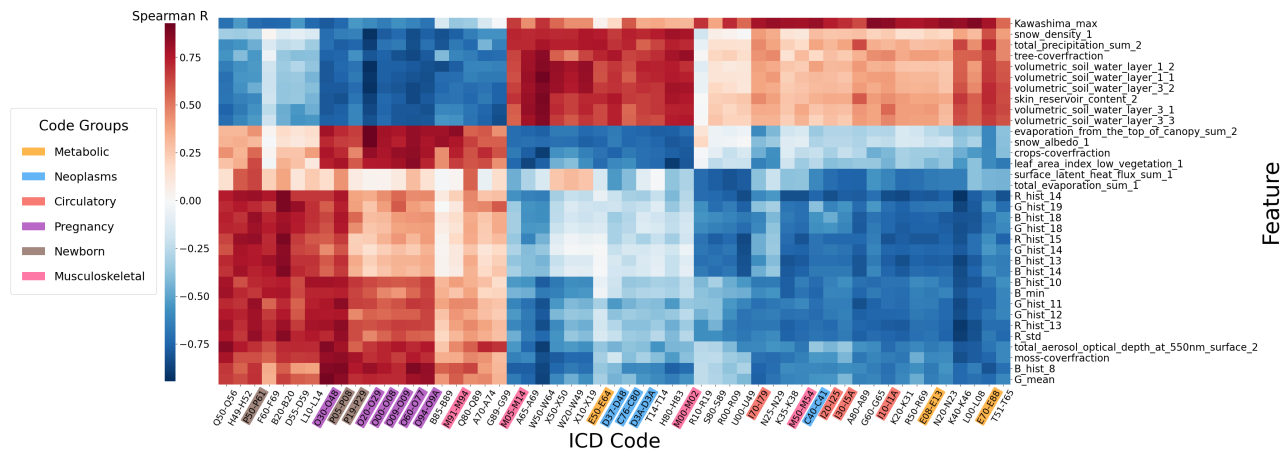


**Figure 2: Feature correlations - second level ICD**

the prevalence of each ICD-10 code for MSAs in a given year by calculating the percentage of patients associated with the code among all patients recorded in that year.

**Data Processing.** The ICD-10 codes are organized hierarchically, allowing for a multi-level investigation of disease prevalence. For instance, the code "I10" represents essential hypertension, its parent node "I10-I1A" represents a broader group of hypertensive diseases, and the top-level code "I00-I99" encompasses circulatory system diseases. This hierarchical structure allows us to explore the prevalence of both broad disease categories and specific conditions. To capture both the overall trends and finer details, we calculated disease prevalence at the top three levels of ICD-10 codes using their first three digits, enabling a comprehensive understanding of disease patterns and correlations.

## 4 Dataset Use Cases

In this section, we first conduct a comprehensive analysis to examine the correlation between environmental data and human health status. We then demonstrate potential use cases of SatHealth through two kinds of tasks: regional public health modeling and personalized disease risk prediction. For regional public health modeling, we use regional environmental embeddings to predict

the SDI score and disease prevalences, which display the power of multimodal data in modeling regional health status. For personalized disease risk prediction, we plug the environmental factors into patient representations produced by EHR risk prediction backbones according to patient residency, which shows the benefits of environmental information in predicting personal disease risks.

### 4.1 Basic Correlation Analysis

We first perform a statistical analysis to analyze the correlation between the living environment and regional disease prevalence. Note that this is a simple illustration of the dataset characteristics instead of a rigorous public health analysis.

**4.1.1 Regional Disparity.** We start by exploring the disparity in health status between regions in Ohio. For a simple illustration, we define Columbus, Cleveland, and Cincinnati as urban areas and compare the disease occurrence with other areas in Ohio. Specifically, we calculate urban-to-rural odds ratios (OR) and their confidence intervals (CI) to show the difference in disease occurrence between the urban (Columbus, Cleveland, and Cincinnati) and other areas.

As Table 3 shows, the urban areas present a significantly higher prevalence of neonatal conditions and pregnancy-related codes.

**Table 4: Regression performance for SDI components and disease prevalence**

Category	Target	MAE ↓				MSE ↓				R <sup>2</sup> ↑			
		DEnv	LC	Img	All	DEnv	LC	Img	All	DEnv	LC	Img	All
SDoH	SDI	<b>0.564</b>	0.621	0.618	<b>0.564</b>	<b>0.461</b>	0.590	0.544	0.464	<b>0.558</b>	0.434	0.478	0.555
	- pct_Poverty_LT100	0.516	<b>0.473</b>	0.480	<b>0.473</b>	0.567	0.424	<b>0.403</b>	0.413	0.277	0.458	<b>0.486</b>	0.473
	- pct_Education_LT12years	<b>0.495</b>	0.600	0.572	0.536	<b>0.526</b>	0.762	0.606	0.552	<b>0.343</b>	0.048	0.243	0.311
	- pct_NonEmployed	0.533	0.593	0.560	<b>0.532</b>	0.740	0.679	0.659	<b>0.577</b>	0.140	0.210	0.234	<b>0.329</b>
	- pct_Single_Parent_Fam	0.509	0.443	<b>0.414</b>	0.433	0.680	0.424	<b>0.369</b>	0.396	-0.285	0.199	<b>0.302</b>	0.251
	- pctHH_No_Vehicle	0.484	0.512	0.519	<b>0.438</b>	0.709	0.743	0.675	<b>0.562</b>	0.406	0.377	0.434	<b>0.529</b>
	- pctHH_Renter_Occupied	0.445	0.462	0.447	<b>0.406</b>	0.382	0.444	0.366	<b>0.315</b>	0.580	0.513	0.598	<b>0.654</b>
	- pctHH_Crowding	0.682	0.709	0.697	<b>0.675</b>	1.113	1.222	1.192	<b>1.052</b>	0.009	-0.089	-0.063	<b>0.062</b>
Disease Prevalence	Neoplasms	0.389	0.392	0.391	<b>0.327</b>	0.284	0.288	0.284	<b>0.215</b>	0.657	0.621	0.632	<b>0.743</b>
	Metabolic diseases	0.424	0.384	0.385	<b>0.366</b>	0.299	0.248	0.250	<b>0.228</b>	0.686	0.706	0.704	<b>0.742</b>
	- Diabetes mellitus	0.295	0.268	0.271	<b>0.267</b>	0.158	0.137	0.139	<b>0.127</b>	0.831	0.848	0.845	<b>0.861</b>
	- Metabolic disorders	0.326	<b>0.249</b>	0.250	0.284	0.195	0.116	<b>0.115</b>	0.142	0.781	0.845	<b>0.846</b>	0.827
	Circulatory system diseases	0.227	0.205	<b>0.200</b>	0.212	0.086	0.075	<b>0.072</b>	0.078	0.900	0.909	<b>0.912</b>	0.909
	- Hypertensive diseases	0.198	0.194	0.186	<b>0.177</b>	0.063	0.062	0.058	<b>0.052</b>	0.928	0.927	0.930	<b>0.939</b>
	- Ischemic heart diseases	0.304	<b>0.249</b>	0.250	0.254	0.185	0.123	<b>0.122</b>	0.142	0.815	0.873	<b>0.874</b>	0.855

All: embeddings by combining all modalities; "-" denotes subcategories

Specifically, the conditions originating in the perinatal period (P00-P96) have an odds ratio of 1.479 (95% CI: 1.418-1.542), and codes for pregnancy, childbirth, and the puerperium (O00-O9A) are also more frequent in urban areas (OR: 1.16, 95% CI: 1.131-1.190). This disparity could have originated from the higher in-hospital ratio of births [69] and limited access to maternity and prenatal care [21, 70, 76].

Moreover, rural areas have more mortality cases with ill-defined and unknown causes (ICD-10: R99, OR: 0.311, 95% CI: 0.227-0.427). This kind of coding is less informative and reflects a relatively lower data quality from the rural healthcare system [47, 72]. Besides, as the US Centers for Disease Control and Prevention (CDC) reported [11], rural residents tend to be older and sicker, and they have higher rates of cigarette smoking, high blood pressure, and obesity. Correspondingly, we observed higher prevalences of circulatory system diseases (I00-I99) as well as Endocrine, nutritional, and metabolic diseases (E00-E89). Specifically, rural areas have higher prevalences for chronic rheumatic heart diseases (OR: 0.631, 95% CI: 0.584-0.681), hypertensive diseases (OR: 0.743, 95% CI: 0.735-0.752), obesity (OR: 0.773, 95% CI: 0.761-0.785), and diabetes (OR: 0.792, 95% CI: 0.778-0.806). We show these results in Tabel 3, and more comprehensive results can be found in Table 10 in supplementary. These findings help us in discovering health inequalities and support policy making [40, 75]. Furthermore, such observations and findings from public health data can help policy development, such as encouraging network development and telemedicine, and improving the rules for Medicare payments to providers [19, 56].

**4.1.2 Factor Correlations.** In addition to the odds ratio, we calculate Spearman’s rank correlation coefficient to investigate the correlation between environmental factors and multi-level ICD code prevalence across spatial regions. We show the pairwise correlations between level-2 ICD codes and environmental features in Figure 2. Note that this figure only shows subsets of ICD codes and features with significant correlations. Additionally, we use color shading on ICD codes to differentiate between disease categories.

More detailed results on a broader set of ICD codes are shown in Figure 6 and 5 in the supplementary results.

We observed several outstanding color blocks in Figure 2, showing groups of diseases with distinct correlations with specific feature subsets. Firstly, a group of newborn or pregnancy-related conditions (O and P codes) with a purple or brown background lies on the left-hand side, with a significant negative correlation with tree cover fraction and volumetric soil water. Such correlation can be a reflection of the higher prevalence of newborn or pregnancy-related conditions in urban areas we found previously, as urban soil tends to be compact with lower water content [52]. In contrast, several neoplasm conditions show the opposite correlation pattern, which reflects a higher prevalence of tumors in rural areas [59]. Moreover, the correlation between neoplasms and soil water may also be explained by the higher mobility of chemical pollutants with higher precipitation and moisturized soil [8].

Moreover, some circulatory system diseases in orange color on the right-hand side, such as hypertensive diseases (I10-I1A) and heart diseases (I30-I5A). A similar pattern also applies to diabetes mellitus (E08-E13) and metabolic disorders (E70-E88). These diseases correlate positively with the Kawashima index [36] and negatively with many satellite image features. As the Kawashima index is negatively correlated to chlorophyll content [61], and image features also provide information about pixel color distribution, these correlations could be explained by the discovered benefit of green space on cardiovascular disease and diabetes [4, 5].

These results highlight the significant impact of the living environment on human health, consistent with existing studies [37, 62, 67]. They also demonstrate the potential of SatHealth to enhance AI models for health-related tasks (e.g., regional public health modeling and personalized disease risk prediction).

**Table 5: Prediction performance of personalized disease risk prediction**

		Next Visit Prediction					1-Year Diagnosis Code Prediction				
		mAUC↑	mAUC-t10↑	Recall@5↑	Recall@10↑	Recall@50↑	mAUC↑	mAUC-t10↑	Recall@5↑	Recall@10↑	Recall@50↑
LSTM	EHR	0.481	0.745	0.240	0.253	0.416	0.487	0.770	<b>0.503</b>	<b>0.537</b>	<b>0.687</b>
	+Env	<b>0.538</b>	<b>0.767</b>	<b>0.288</b>	<b>0.325</b>	<b>0.561</b>	<b>0.551</b>	<b>0.815</b>	0.489	0.508	0.642
RETAIN	EHR	0.476	0.678	<b>0.273</b>	<b>0.301</b>	<b>0.456</b>	0.492	0.703	0.198	0.221	0.463
	+Env	<b>0.551</b>	<b>0.816</b>	<b>0.273</b>	0.287	0.445	<b>0.543</b>	<b>0.764</b>	<b>0.205</b>	<b>0.265</b>	<b>0.503</b>
Dipole	EHR	0.600	0.869	0.263	0.302	0.487	0.660	0.929	0.477	0.504	0.641
	+Env	<b>0.722</b>	<b>0.942</b>	<b>0.416</b>	<b>0.480</b>	<b>0.724</b>	<b>0.734</b>	<b>0.932</b>	<b>0.553</b>	<b>0.587</b>	<b>0.769</b>
Transformer	EHR	0.484	0.679	0.215	0.240	0.439	0.503	0.706	0.310	0.333	0.523
	+Env	<b>0.549</b>	<b>0.738</b>	<b>0.234</b>	<b>0.265</b>	<b>0.495</b>	<b>0.553</b>	<b>0.732</b>	<b>0.341</b>	<b>0.377</b>	<b>0.584</b>

## 4.2 Regional Public Health Modeling

Regional public health modeling aims to predict health outcomes for the community or regional population. It helps identify health disparities and guide targeted interventions to improve public health outcomes and resource allocation [40, 75]. In this subsection, we use the created regional environment embeddings to predict regional SDI and disease prevalence to reveal the relationship between living environment and population health status.

We divide the environmental features into two subsets according to data structure: (1) **Dynamic environmental factors (DEnv)** refers to environmental factors that change over time, including climate, air quality, and greenery variables; (2) **Static environmental factors** refers to environmental factors that are stable over time, which include **Land Cover (LC)** and **Satellite images (Img)**. For baselines, we train random forest regressors respectively on the feature subsets to show their fundamental functional relevance. After that, we combine all modalities (**All**) and display how this helps in regional health status modeling.

**4.2.1 SDoH Regression.** The upper part of Table 4 presents the performance of the Social Deprivation Index (SDI) prediction. The performance metrics include Mean Absolute Error (MAE), Mean Squared Error (MSE), and  $R^2$ , providing a comprehensive assessment of model accuracy and explanatory power. It is worth pointing out that we normalize the prevalence target by z-score normalization such that they have a standardized deviation of 1.

**Overall SDI.** When predicting overall SDI, the dynamic features (DEnv) achieve the best performance, yielding the lowest MAE and highest  $R^2$ . Besides, the combined feature (All) performs slightly worse but is comparable to DEnv, suggesting that DEnv variables predominantly drive the prediction. In contrast, land cover and image embeddings show suboptimal performance, likely because they capture only ground-level views, making it challenging to predict a comprehensive socioeconomic score.

**Population Characteristics** include poverty, education, and employment status. In this category, the best-performing features vary, suggesting different dependencies of SDoH on environmental factors. Specifically, the poverty ratio is better predicted by image features, likely due to their ability to capture urban-rural disparities, such as housing conditions. Education status relies more on dynamic features (*i.e.*, climate, greenery, air quality). Employment benefits most from multimodal fusion as a combination of economic, infrastructure, and environmental factors influences it.

**Household Characteristics** refer to household-level factors, including single-parent family percentage, housing tenure (rent or owner-occupied), vehicle ownership, and household crowdedness. The combined feature outperforms all other features in predicting household characteristics except for the single-parent family ratio. This superiority indicates that integrating multimodal features provides a more comprehensive understanding of housing-related metrics. The combined features perform poorly in predicting the single-parent family ratio, likely because dynamic features (DEnv) tend to be independent of family structure. However, it is worth noting that none of these features are effective predictors for crowding prediction, with the best  $R^2$  score around 0.06.

**4.2.2 Disease Prevalence Regression.** There are thousands of diseases, but only a small subset correlates significantly with environmental features. Therefore, we focus on diseases reported to correlate with environmental factors [4, 5]: neoplasms (C00-D49), endocrine, nutritional, and metabolic diseases (E00-E89), and circulatory system diseases (I00-I99). Moreover, we explored several subcategories, including diabetes (E08-E13), metabolic disorders (E70-E88), hypertensive diseases (I10-I1A), and ischemic heart diseases (I20-I25).

**Overall Comparison.** We show the regression performance of predicting the prevalence of the diseases in the lower part of Table 4. For most diseases (*e.g.*, Neoplasms and Metabolic diseases), combining all modalities (All) achieves the best prediction performance, demonstrating the essential role of multimodal environmental factors in modeling the regional prevalence of these diseases.

**Neoplasms.** Neoplasms (C00-D49) include all kinds of tumors, including both malignant and benign. Table 4 shows that dynamic features (DEnv) have better prediction performance than land cover and satellite, as these features contain carcinogens potentially related to some specific cancer, such as solar radiation [4] and air pollutants [68]. Moreover, by combining all features, the regression model gains 0.086 improvement in  $R^2$ , the highest improvement among the explored diseases. Such improvement demonstrates that the three feature sets are complementary when modeling neoplasm prevalence.

**Metabolic diseases.** As for endocrine, nutritional, and metabolic diseases (E00-E89), land cover (LC) and satellite image (Img) features perform consistently better than dynamic factors (DEnv). Especially for metabolic disorders (E70-E88), the  $R^2$  score on dynamic factors is 0.064 lower than the other two features. This is intuitively reasonable as these diseases are more related to our

**Table 6: Model  $R^2$  scores for Spatiotemporal Generalization. Bold: best results, underlined: second best.**

Features	Spa. In.		Spa. Ex.		Temp. For.
	SDoH	Prev.	SDoH	Prev.	Prev.
DEnv	0.183	0.667	-0.186	0.552	0.811
DEnv + T	0.161	0.665	-0.301	0.522	0.868
DEnv + S	0.183	0.705	-0.261	0.552	0.759
DEnv + T + S	0.165	<b>0.711</b>	-0.296	<b>0.624</b>	0.820
All	0.244	0.665	<b>0.035</b>	0.543	0.902
All + T	0.238	0.671	-0.005	0.525	<b>0.928</b>
All + S	<b>0.275</b>	0.699	0.014	0.572	0.879
All + T + S	<u>0.265</u>	<u>0.709</u>	<u>0.026</u>	<u>0.619</u>	0.914

Prev.: Disease Prevalence; Spa.: Spatial; Temp.: Temporal;  
Ex.: extrapolation; In.: interpolation; For.: forecasting

lifestyle [38, 55], and the effect of air quality or climate tends to be long-term and maybe implicit [82].

**Circulatory system diseases.** Finally, it can be seen that the three feature modalities gain high but similar performance for circulatory system diseases (I00-I99), and the improvement of combined features is not significant. This could be due to each feature modality’s relatively high performance, making it hard to improve further. On the other hand, land cover (LC) and satellite features (Img) have higher performances than dynamic factors (DEnv) for ischemic heart diseases (I20-I25), possibly due to the reported correlation between green space and ischemic heart diseases [5].

### 4.3 Personalized Disease Risk Prediction

In this subsection, we use living environmental data to help predict patient-level disease risks. Specifically, we focus on the next visit prediction and 1-year predictive modeling tasks. We use the patient visit history data from the MarketScan database [13] to conduct experiments. We build models to predict the level-2 ICD codes within a patient visit with all previous visits from the patient. We define the multi-label ground truth in two ways: **Next visit** setting takes the codes from one patient as ground truth no matter how long it is from the patient’s last visit, while **1-Year Predictive Modeling** setting takes all code within the next one year of the patient’s last known visit. In addition to patients’ visit history, we concatenate the embedding of the patient’s living environment to the patient representation produced by the visit encoder network to enhance the backbone model. The embedding of the patient’s living environment is created by data within the patient’s residence area in the year of the patient’s last known visit.

We implemented several backbone networks for comparison. They are well-known architectures handling sequences, including LSTM [32] and Transformer [66], and models designed for medical data such as RETAIN [17] and Dipole [43]. This task can be formulated as a multi-label problem, so we use the macro average AUROC score (mAUC) across all diseases as the basic evaluation metric. Additionally, we use the macro average AUROC score of the top 10 performed diseases (mAUC-t10). Furthermore, as this model predicts the disease risk for each patient, we calculate the

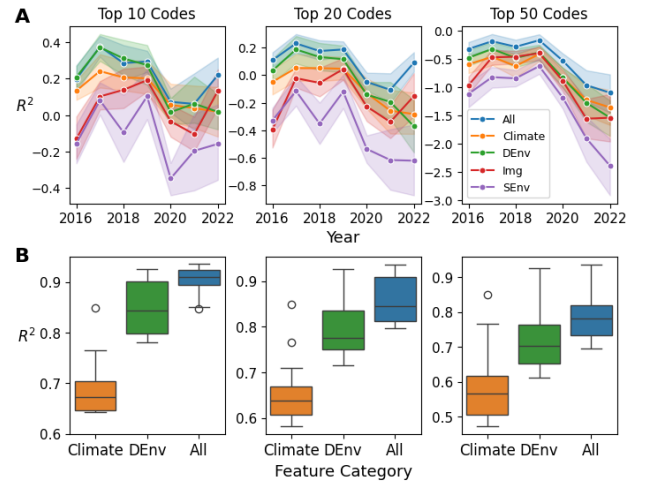


**Figure 3: Random Forest Regression Performance from Different Feature Groups. (A)  $R^2$  score per year for spatial interpolation. (B)  $R^2$  score for temporal extrapolation.**

recall at k (Recall@k) metric to evaluate the model’s capability of producing correct disease warnings for patients.

We put the experimental results in Table 5. We highlight the best performance among two variations in bold for each backbone model. Using environmental information boosts model performance in most cases, especially for the recall, indicating that the patient’s living environment may help us identify their disease risks. Moreover, for the next visit prediction task, models with environmental information tend to have much higher mAUC scores for top-performed diseases, which shows the capability of environmental data in differentiating patients with various disease risks.

### 4.4 Spatiotemporal Generalizability Analysis

The living environment varies in different areas and is subject to change over time. Therefore, users must be careful about spatiotemporal distribution shifts when applying models trained on SatHealth to other regions or conducting long-term forecasting. To find out how this affects the model performance with SatHealth, we conducted experiments on three cases of spatiotemporal generalization on regional public health modeling. Moreover, we designed a spatiotemporal-enhanced regression strategy to improve model robustness. In this subsection, we show the experimental performance of the enhanced model in the three generalization scenarios: spatial interpolation (e.g., missing value imputation [6]), spatial extrapolation (e.g., distant region generalization [46, 54]), and temporal forecasting [31, 51]. We provide more experimental details in the supplementary Section C.1.

We start by evaluating the generalizability of basic regression models without spatiotemporal enhancements. Using  $R^2$  scores, we show the top 10, 20, and 50 performing diseases. Figure 3 compares model performance across input modalities for (A) spatial interpolation and (B) temporal forecasting. LC and Img models are excluded from temporal forecasting due to their time independence. A model trained solely on climate variables is also included for

comparison. For spatial interpolation, we stratify results by year. As shown in Figure 3B, Combined features show higher stability to temporal shift, likely due to reduced feature variance over time. Additionally, the combined features improve spatial generalization. Dynamic features, including climate, greenery, and air quality, exhibit stronger spatial robustness, possibly due to their pronounced spatial clustering effect.

Next, we show how spatiotemporal information can improve model generalizability. We train boosting models as described in Section C.1.2. Models with neighborhood information are annotated with "+S", and models with history information are annotated with "+T". We compared the combined feature model (All) with the Dynamic feature model (DEnv) on both SDoH and disease prevalence regression under three generalization cases, and the result is shown in Table 6. It can be seen that incorporating spatiotemporal information can be beneficial to model robustness, as the "+T+S" models are either the best or the second best for all cases. Although not the best, the "All+T+S" model is comparable to the best, providing a general solution that works under all cases. Moreover, the combined feature models tend to perform better than the DEnv models, further showing the multimodal models' benefits. Finally, we find that our model performs poorly when predicting SDoH under spatial extrapolation, which may indicate a high spatial disparity between regions, making the spatial generalization of the SDoH model challenging.

## 5 Web Application Deployment

To improve the utility of our dataset, we designed a web-based application to explore and access SatHealth. The system design is shown in Figure 4.

The default page (Figure 4A) is the satellite map of Ohio, with the overall SDI score for each county shown in the heatmap. Users can select different variables to be displayed in the heatmap, including SDI, environmental variables, and disease prevalence of the user-selected ICD code. For time-dependent variables, there's a slide bar for users to define the time range of the data shown. Moreover, diseases with a high correlation to environmental features are shown below the map; users can also select specific environmental features to check their correlation to the map. We also provide the button to download the whole dataset at the top of this page. More information about data access can be found in Section A.4.

Once users click on one of the regions in the map, its basic information will be shown in a new column on the right-hand side (Figure 4B). There will be three sub-panels in this sidebar. On the top, basic metrics, including population and total area of the region, are shown, together with the overall SDI score and seasonal average temperature. When users click the "Show Details" button, a drop-down list will appear to display more variables. Buttons are also provided to download the SatHealth subset in the selected region. In the middle, there's a list of the most prevalent diseases in the selected region; users can also search for ICD codes to see their prevalence. At the bottom of this sidebar, random satellite images in the selected region will be displayed.

Users can check the selection box in the disease list. The right-hand side column will be updated (Figure 4C) to show a bar chart of the correlation score of the selected disease with the top 5 correlated

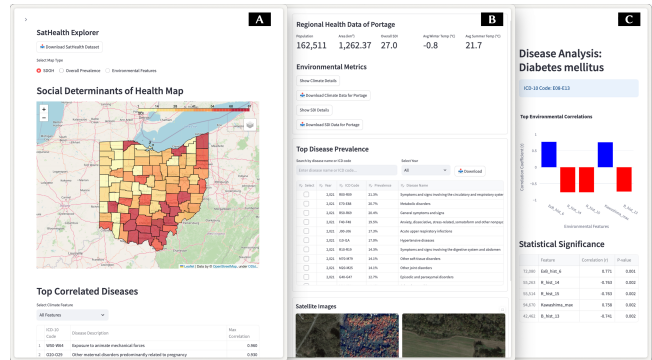


Figure 4: UI design of the proposed dataset

environmental features in a bar chart. The correlation score and corresponding p-value will also be displayed below the bar chart. Users can search for a specific variable to check its correlation to the current disease.

## 6 Limitations and Future Work

Our work still has several limitations. First, SatHealth is currently restricted to Ohio due to budget constraints, but we will gradually expand our dataset to include more states, toward full US coverage. Furthermore, although environmental data showed effectiveness in our experiment, our embedding method of such multimodal data is relatively straightforward using feature engineering. We will explore more complicated deep-learning strategies to unlock the power of multimodal environmental data. Finally, the individual residences in our dataset are coarse due to privacy issues, making the living environment less representative. Despite these limitations, we believe SatHealth still provides a solid foundation and a good starting point for research on the interplay between the living environment and human health.

## 7 Conclusion

In this study, we developed SatHealth, a multimodal public dataset in Ohio consisting of environmental variables, satellite images, SDoH, and regional disease prevalence. To the best of our knowledge, SatHealth is the first dataset in the US that combines regional environmental characteristics with a healthcare database. We designed an embedding pipeline to fuse multimodal environmental data and produce regional living environment representations. Using the representation, we conduct experiments on two tasks: regional public health modeling and personalized disease risk prediction. The experimental results show that multimodal environmental information helps boost model performance in these problems. We also find that leveraging spatiotemporal information helps improve model robustness. Finally, we deployed a web application for users to explore and download our dataset.

## Acknowledgments

We acknowledge the funding for the project provided by the National Institute of Allergy and Infectious Diseases (R01AI188576), the National Institute on Drug Abuse (R01DA057668), and the National Science Foundation (2145625).

## References

- [1] European Space Agency. 2024. *Sentinel-2*. <https://sentinewiki.copernicus.eu/web/sentinel-2>
- [2] Suraiya P Ahmad, Omar Torres, Pawan K Bhartia, Gregory Leptoukh, and SJ Kempler. 2006. Aerosol index from TOMS and OMI measurements. In *Proc. of the 86th AMS annual meeting*.
- [3] Leonardo D. Araújo, Daniel C. Zanotta, Nicolas Ray, and Mauricio R. Veronez. 2024. Earth observation data uncover green spaces' role in mental health. *Scientific Reports* 14, 1 (Sept. 2024), 20933. doi:10.1038/s41598-024-72008-8 Publisher: Nature Publishing Group.
- [4] Aji Kusumaning Asri, Chia-Pin Yu, Wen-Chi Pan, Yue Leon Guo, Huey-Jen Su, Shih-Chun Candice Lung, Chih-Da Wu, and John D Spengler. 2020. Global greenness in relation to reducing the burden of cardiovascular diseases: ischemic heart disease and stroke. *Environmental Research Letters* 15, 12 (Dec. 2020), 124003. doi:10.1088/1748-9326/abbaf
- [5] Thomas Astell-Burt and Xiaojiao Feng. 2019. Urban green space, tree canopy, and prevention of heart disease, hypertension, and diabetes: a longitudinal study. *The Lancet Planetary Health* 3 (Sept. 2019), S16. doi:10.1016/S2542-5196(19)30159-7 Publisher: Elsevier.
- [6] Jannah Baker, Nicole White, and Kerrie Mengersen. 2014. Missing in space: an evaluation of imputation methods for missing data in spatial analysis of risk factors for type II diabetes. *International Journal of Health Geographics* 13, 1 (Nov. 2014), 47. doi:10.1186/1476-072X-13-47
- [7] Evelise Pereira Barboza, Marta Cirach, Sasha Khomenko, Tamara Iungman, Natalie Mueller, Jose Barrera-Gómez, David Rojas-Rueda, Michelle Kondo, and Mark Nieuwenhuijsen. 2021. Green space and mortality in European cities: a health impact assessment study. *The Lancet Planetary Health* 5, 10 (Oct. 2021), e718–e730. doi:10.1016/S2542-5196(21)00229-1
- [8] Bhabananda Biswas, Fangjie Qi, Jayanta Kumar Biswas, Ayanka Wijayawardena, Muhammad Atikul Islam Khan, and Ravi Naidu. 2018. The Fate of Chemical Pollutants with Soil Properties and Processes in the Climate Change Paradigm—A Review. *Soil Systems* 2, 3 (Sept. 2018), 51. doi:10.3390/soilsystems2030051 Number: 3 Publisher: Multidisciplinary Digital Publishing Institute.
- [9] US Census Bureau. 2024. *American Community Survey (ACS)*. <https://www.census.gov/programs-surveys/acs> Section: Government.
- [10] Xiaofeng Cao, Yulin Liu, Rui Yu, Dejun Han, and Baofeng Su. 2021. A Comparison of UAV RGB and Multispectral Imaging in Phenotyping for Stay Green of Wheat Population. *Remote Sensing* 13, 24 (Dec. 2021), 5173. doi:10.3390/rs13245173
- [11] CDC. 2024. About Rural Health. Retrieved 2025-01-16 from <https://www.cdc.gov/rural-health/php/about/index.html>
- [12] CDC. 2024. *ICD-10-CM*. <https://www.cdc.gov/nchs/icd/icd-10-cm/index.html>
- [13] Jiayuan Chen, Changchang Yin, Yuanlong Wang, and Ping Zhang. 2024. Predictive Modeling with Temporal Graphical Representation on Electronic Health Records. doi:10.48550/arXiv.2405.03943 arXiv:2405.03943 [cs].
- [14] Zhuo Chen, Jean-Eudes Dazard, Yassin Khalifa, Issam Motairek, Sadeer Al-Kindi, and Sanjay Rajagopalan. 2024. Artificial intelligence-based assessment of built environment from Google Street View and coronary artery disease prevalence. *European Heart Journal* 45, 17 (May 2024), 1540–1549. doi:10.1093/eurheartj/ehae158
- [15] Zhuo Chen, Jean-Eudes Dazard, Yassin Khalifa, Issam Motairek, Catherine Kreatsoulas, Sanjay Rajagopalan, and Sadeer Al-Kindi. 2024. Deep Learning-Based Assessment of Built Environment From Satellite Images and Cardiometabolic Disease Prevalence. *JAMA Cardiology* 9, 6 (June 2024), 556. doi:10.1001/jamacardio.2024.0749
- [16] Edward Choi, Mohammad Taha Bahadori, Le Song, Walter F. Stewart, and Jimeng Sun. 2017. GRAM: Graph-based Attention Model for Healthcare Representation Learning. In *Proceedings of the 23rd ACM SIGKDD International Conference on Knowledge Discovery and Data Mining (KDD '17)*. Association for Computing Machinery, New York, NY, USA, 787–795. doi:10.1145/3097983.3098126
- [17] Edward Choi, Mohammad Taha Bahadori, Jimeng Sun, Joshua Kulas, Andy Schuetz, and Walter Stewart. 2016. RETAIN: An Interpretable Predictive Model for Healthcare using Reverse Time Attention Mechanism. In *Advances in Neural Information Processing Systems*, Vol. 29. Curran Associates, Inc. <https://proceedings.neurips.cc/paper/2016/hash/231141b34c82aa95e48810a9d1b33a79-Abstract.html>
- [18] Anne Cleary, Anne Roiko, Nicola W. Burton, Kelly S. Fielding, Zoe Murray, and Gavin Turrell. 2019. Changes in perceptions of urban green space are related to changes in psychological well-being: Cross-sectional and longitudinal study of mid-aged urban residents. *Health & Place* 59 (Sept. 2019), 102201. doi:10.1016/j.healthplace.2019.102201
- [19] Steven S. Coughlin, Catherine Clary, J. Aaron Johnson, Adam Berman, Vahe Heboyan, Teal Benevides, Justin Moore, and Varghese George. 2019. Continuing Challenges in Rural Health in the United States. *Journal of environment and health sciences* 5, 2 (2019), 90–92. <https://www.ncbi.nlm.nih.gov/pmc/articles/PMC7043306/>
- [20] Payam Dadvand, John Wright, David Martinez, Xavier Basagaña, Rosemary R.C. McEachan, Marta Cirach, Christopher J. Gidlow, Kees De Hoogh, Regina Gražulevičienė, and Mark J. Nieuwenhuijsen. 2014. Inequality, green spaces, and pregnant women: Roles of ethnicity and individual and neighbourhood socioeconomic status. *Environment International* 71 (Oct. 2014), 101–108. doi:10.1016/j.envint.2014.06.010
- [21] Natalie A. DiPietro Mager, Terrell W. Zollinger, Jack E. Turman, Jianjun Zhang, and Brian E. Dixon. 2021. Routine Healthcare Utilization Among Reproductive-Age Women Residing in a Rural Maternity Care Desert. *Journal of Community Health* 46, 1 (Feb. 2021), 108–116. doi:10.1007/s10900-020-00852-6
- [22] Haikuan Feng, Huilin Tao, Zhenhai Li, Guijun Yang, and Chunjiang Zhao. 2022. Comparison of UAV RGB Imagery and Hyperspectral Remote-Sensing Data for Monitoring Winter Wheat Growth. *Remote Sensing* 14, 15 (Aug. 2022), 3811. doi:10.3390/rs14153811
- [23] Soledad Fernández. 2024. *Opioid and SUD Data Enclave (O-SUDDen): Bringing real-time data to the opioid crisis*. <https://reporter.nih.gov/project-details/10590246>
- [24] Sebastien Garrigues, Julien Chimot, Melanie Ades, Antje Inness, Johannes Flemming, Zak Kipling, Istvan Laszlo, Angela Benedetti, Roberto Ribas, Soheila Fariserajehlou, et al. 2022. Monitoring multiple satellite aerosol optical depth (AOD) products within the Copernicus Atmosphere Monitoring Service (CAMS) data assimilation system. *Atmospheric Chemistry and Physics* 22, 22 (2022), 14657–14692.
- [25] Mireia Gascon, Margarita Triguero-Mas, David Martinez, Payam Dadvand, David Rojas-Rueda, Antoni Plasencia, and Mark J. Nieuwenhuijsen. 2016. Residential green spaces and mortality: A systematic review. *Environment International* 86 (Jan. 2016), 60–67. doi:10.1016/j.envint.2015.10.013
- [26] Rory Gibb, Felipe J. Colón-González, Phan Trong Lan, Phan Thi Huong, Vu Sinh Nam, Vu Trong Duoc, Do Thai Hung, Nguyen Thanh Dong, Vien Chinh Chien, Ly Thi Thuy Trang, Do Kien Quoc, Tran Minh Hoa, Nguyen Huu Tai, Tran Thi Hang, Gina Tsarouchi, Eleanor Ainscoe, Quillon Harpham, Barbara Hofmann, Darren Lumbroso, Oliver J. Brady, and Rachel Lowe. 2023. Interactions between climate change, urban infrastructure and mobility are driving dengue emergence in Vietnam. *Nature Communications* 14, 1 (Dec. 2023), 8179. doi:10.1038/s41467-023-43954-0
- [27] Michael F. Goodchild and Wenwen Li. 2021. Replication across space and time must be weak in the social and environmental sciences. *Proceedings of the National Academy of Sciences* 118, 35 (Aug. 2021), e2015759118. doi:10.1073/pnas.2015759118
- [28] Google. 2024. *Google Maps Static API*. <https://developers.google.com/maps/documentation/maps-static/overview>
- [29] Noel Gorelick, Matt Hancher, Mike Dixon, Simon Ilyushchenko, David Thau, and Rebecca Moore. 2017. Google Earth Engine: Planetary-scale geospatial analysis for everyone. *Remote Sensing of Environment* 202 (Dec. 2017), 18–27. doi:10.1016/j.rse.2017.06.031
- [30] Christelle Gée and Emmanuel Denimal. 2020. RGB Image-Derived Indicators for Spatial Assessment of the Impact of Broadleaf Weeds on Wheat Biomass. *Remote Sensing* 12, 18 (Sept. 2020), 2982. doi:10.3390/rs12182982
- [31] Kyle Heuton, Jyontika Kapoor, Shikhar Shrestha, Thomas J Stopka, and Michael C Hughes. 2024. Spatiotemporal Forecasting of Opioid-Related Fatal Overdoses: Towards Best Practices for Modeling and Evaluation. *American Journal of Epidemiology* (Sept. 2024), kwae343. doi:10.1093/aje/kwae343
- [32] Sepp Hochreiter and Jürgen Schmidhuber. 1997. Long Short-Term Memory. *Neural Comput.* 9, 8 (1997), 1735–1780. doi:10.1162/neco.1997.9.8.1735
- [33] Pawinee Iamtrakul, Sarad Chayphong, Sajjakaj Jomnonkwa, and Vatanavongs Ratanavaraha. 2021. The Association of Falls Risk in Older Adults and Their Living Environment: A Case Study of Rural Area, Thailand. *Sustainability* 13, 24 (Dec. 2021), 13756. doi:10.3390/su132413756
- [34] Robert Graham Center Policy Studies in Family Medicine & Primary Care. 2018. *Social Deprivation Index (SDI)*. Retrieved 2024-11-19 from <https://www.graham-center.org/content/brand/rgc/maps-data-tools/social-deprivation-index.html>
- [35] J Irizar, M Melf, P Bartsch, J Koehler, S Weiss, R Greinacher, M Erdmann, V Kirschner, A Perez Albinana, and D Martin. 2019. Sentinel-5/uvns. In *International Conference on Space Optics—ICSO 2018*, Vol. 11180. SPIE, 41–58.
- [36] SHIGETO KAWASHIMA and MAKOTO NAKATANI. 1998. An Algorithm for Estimating Chlorophyll Content in Leaves Using a Video Camera. *Annals of Botany* 81, 1 (Jan. 1998), 49–54. doi:10.1006/anbo.1997.0544
- [37] Katherine Keenan, Michail Papatthomas, Stephen E. Mshana, Benon Asiimwe, John Kiiru, Andy G. Lynch, Mike Kesby, Stella Neema, Joseph R. Mwanga, Martha F. Mushi, Wei Jing, Dominique L. Green, Emmanuel Olamijuwon, Qing Zhang, Rachel Sippy, Kathryn J. Fredricks, Stephen H. Gillespie, Wilber Sabiti, Joel Bazira, Derek J. Sloan, Blandina T. Mmbaga, Gibson Kibiki, David Aanensen, John Stelling, V. Anne Smith, Alison Sandeman, and Matthew T. G. Holden. 2024. Intersecting social and environmental determinants of multidrug-resistant urinary tract infections in East Africa beyond antibiotic use. *Nature Communications* 15, 1 (Oct. 2024), 9418. doi:10.1038/s41467-024-53253-x
- [38] Thao Minh Lam, Nicolette R. den Braver, and Jeroen Lakerveld. 2023. The Built Environment and Metabolic Syndrome. In *Metabolic Syndrome: A Comprehensive*

- Textbook, Rexford S. Ahima (Ed.). Springer International Publishing, Cham, 217–228. doi:10.1007/978-3-031-40116-9\_59
- [39] Xiaotong Li, Lihua Li, Wen Qin, Qing Cao, Xin Mu, Tiange Liu, Zhen Li, and Wei Zhang. 2023. Urban Living Environment and Myopia in Children. *JAMA Network Open* 6, 12 (Dec. 2023), e2346999. doi:10.1001/jamanetworkopen.2023.46999
- [40] Eméfah C. Locooh, Maddox Karen E. Joynt, Yun Wang, Dhruv S. Kazi, Robert W. Yeh, and Rishi K. Wadhera. 2022. Rural-Urban Disparities in Outcomes of Myocardial Infarction, Heart Failure, and Stroke in the United States. *Journal of the American College of Cardiology* 79, 3 (Jan. 2022), 267–279. doi:10.1016/j.jacc.2021.10.045 Publisher: American College of Cardiology Foundation.
- [41] Jiajun Luo, Rena R. Jones, Zhihao Jin, Tamar Polonsky, Karen Kim, Christopher O. Olopade, Jayant Pinto, Habibul Ahsan, and Briseis Aschebrook-Kilfoy. 2024. Differing associations of PM<sub>2.5</sub> exposure with systolic and diastolic blood pressures across exposure durations in a predominantly non-Hispanic Black cohort. *Scientific Reports* 14, 1 (Aug. 2024), 20256. doi:10.1038/s41598-024-64851-6
- [42] Junyu Luo, Muchao Ye, Cao Xiao, and Fenglong Ma. 2020. HiTANet: Hierarchical Time-Aware Attention Networks for Risk Prediction on Electronic Health Records. In *Proceedings of the 26th ACM SIGKDD International Conference on Knowledge Discovery & Data Mining*. ACM, Virtual Event CA USA, 647–656. doi:10.1145/3394486.3403107
- [43] Fenglong Ma, Radha Chitta, Jing Zhou, Quanzeng You, Tong Sun, and Jing Gao. 2017. Dipole: Diagnosis Prediction in Healthcare via Attention-based Bidirectional Recurrent Neural Networks. In *Proceedings of the 23rd ACM SIGKDD International Conference on Knowledge Discovery and Data Mining*. ACM, Halifax NS Canada, 1903–1911. doi:10.1145/3097983.3098088
- [44] Fenglong Ma, Quanzeng You, Houping Xiao, Radha Chitta, Jing Zhou, and Jing Gao. 2018. KAME: Knowledge-based Attention Model for Diagnosis Prediction in Healthcare. In *Proceedings of the 27th ACM International Conference on Information and Knowledge Management*. ACM, Torino Italy, 743–752. doi:10.1145/3269206.3271701
- [45] Merative. 2024. *Real world evidence*. <https://www.merative.com/real-world-evidence>
- [46] Hanna Meyer and Edzer Pebesma. 2021. Predicting into unknown space? Estimating the area of applicability of spatial prediction models. *Methods in Ecology and Evolution* 12, 9 (2021), 1620–1633. doi:10.1111/2041-210X.13650 \_eprint: <https://onlinelibrary.wiley.com/doi/pdf/10.1111/2041-210X.13650>
- [47] Lene Mikkelsen, Kim Moesgaard Iburg, Tim Adair, Thomas Fürst, Michael Hegnauer, Elena von der Lippe, Lauren Moran, Shuhei Nomura, Haruka Sakamoto, Kenji Shibuya, Annelene Wengler, Stephanie Willbond, Patricia Wood, and Alan D. Lopez. 2020. Assessing the quality of cause of death data in six high-income countries: Australia, Canada, Denmark, Germany, Japan and Switzerland. *International Journal of Public Health* 65, 1 (Jan. 2020), 17–28. doi:10.1007/s00038-019-01325-x
- [48] Dana Moukheiber, David Restrepo, Sebastián Andrés Cajas, María Patricia Arbeláez Montoya, Leo Anthony Celi, Kuan-Ting Kuo, Diego M. López, Lama Moukheiber, Mira Moukheiber, Sulaiman Moukheiber, Juan Sebastian Osorio-Valencia, Saptarshi Purkayastha, Atika Rahman Paddo, Chenwei Wu, and Po-Chih Kuo. 2024. A multimodal framework for extraction and fusion of satellite images and public health data. *Scientific Data* 11, 1 (June 2024), 634. doi:10.1038/s41597-024-03366-1
- [49] J. Muñoz Sabater. 2024. *ERA5-Land hourly data from 1950 to present*. <https://cds.climate.copernicus.eu/datasets/reanalysis-era5-land?tab=overview>
- [50] Nushrat Nazia, Jane Law, and Zahid Ahmad Butt. 2022. Identifying spatiotemporal patterns of COVID-19 transmissions and the drivers of the patterns in Toronto: a Bayesian hierarchical spatiotemporal modelling. *Scientific Reports* 12, 1 (June 2022), 9369. doi:10.1038/s41598-022-13403-x
- [51] Behnam Nikparvar, Md Mokhlesur Rahman, Faizeh Hatami, and Jean-Claude Thill. 2021. Spatio-temporal prediction of the COVID-19 pandemic in US counties: modeling with a deep LSTM neural network. *Scientific Reports* 11, 1 (Nov. 2021), 21715. doi:10.1038/s41598-021-01119-3 Publisher: Nature Publishing Group.
- [52] U.S. Department of Agriculture (USDA). 2025. Urban Soil Survey | Natural Resources Conservation Service. Retrieved 2025-01-21 from <https://www.nrcs.usda.gov/conservation-basics/natural-resource-concerns/soil/urban-soil-survey>
- [53] U.S. Department of Health, Office of Disease Prevention Human Services, and Health Promotion. 2024. *Social Determinants of Health - Healthy People 2030 | odphp.health.gov*. Retrieved 2024-11-19 from <https://odphp.health.gov/healthypeople/priority-areas/social-determinants-health>
- [54] Allison P. Patton, Wig Zamore, Elena N. Naumova, Jonathan I. Levy, Doug Brugge, and John L. Durant. 2015. Transferability and Generalizability of Regression Models of Ultrafine Particles in Urban Neighborhoods in the Boston Area. *Environmental Science & Technology* 49, 10 (May 2015), 6051–6060. doi:10.1021/es5061676 Publisher: American Chemical Society.
- [55] Muhammad Mainuddin Patwary, Mohammad Javad Zare Sakhvidi, Sadia Ashraf, Payam Davdand, Matthew H. E. M. Browning, Md Ashraf Alam, Michelle L. Bell, Peter James, and Thomas Astell-Burt. 2024. Impact of green space and built environment on metabolic syndrome: A systematic review with meta-analysis. *Science of The Total Environment* 923 (May 2024), 170977. doi:10.1016/j.scitotenv.2024.170977
- [56] Thomas C. Ricketts. 2000. The Changing Nature of Rural Health Care. *Annual Review of Public Health* 21, 1 (May 2000), 639–657. doi:10.1146/annurev.publhealth.21.1.639
- [57] David R. Roberts, Volker Bahn, Simone Ciuti, Mark S. Boyce, Jane Elith, Gurutzeta Guillera-Arroita, Severin Hauenstein, José J. Lahoz-Monfort, Boris Schröder, Wilfried Thuiller, David I. Warton, Brendan A. Wintle, Florian Hartig, and Carsten F. Dormann. 2017. Cross-validation strategies for data with temporal, spatial, hierarchical, or phylogenetic structure. *Ecography* 40, 8 (2017), 913–929. doi:10.1111/ecog.02881
- [58] Sanja Scepanovic, Ivica Obadic, Sagar Joglekar, Laura Giustarini, Cristiano Nattero, Daniele Quercia, and Xiaoxiang Zhu. 2024. MedSat: A Public Health Dataset for England Featuring Medical Prescriptions and Satellite Imagery. *Advances in Neural Information Processing Systems* 36 (2024).
- [59] Jason Semprini, Khyathi Gadag, Gawain Williams, Aniyah Mldrow, and Whitney E. Zahnd. 2024. Rural-Urban Cancer Incidence and Trends in the United States, 2000 to 2019. *Cancer Epidemiology, Biomarkers & Prevention* 33, 8 (Aug. 2024), 1012–1022. doi:10.1158/1055-9965.EPI-24-0072
- [60] Copernicus Land Monitoring Service. 2024. *Dynamic Land Cover*. <https://land.copernicus.eu/en/products/global-dynamic-land-cover>
- [61] Santiago Signorelli, Esteban Casaretto, and A. Harvey Millar. 2023. Green Index: a widely accessible method to quantify greenness of photosynthetic organisms. doi:10.1101/2023.08.23.554481
- [62] Adrian Spoerri, Marcel Zwahlen, Matthias Egger, and Matthias Bopp. 2010. The Swiss National Cohort: a unique database for national and international researchers. *International Journal of Public Health* 55, 4 (Aug. 2010), 239–242. doi:10.1007/s00038-010-0160-5
- [63] Kai Sun, Yingjie Hu, Gaurish Lakhnpal, and Ryan Zhenqi Zhou. 2023. Spatial cross-validation for GeoAI. In *Handbook of Geospatial Artificial Intelligence*. CRC Press, 201–214.
- [64] Anastasios Temenos, Ioannis N. Tzortzis, Maria Kaselimi, Ioannis Rallis, Anastasios Doulamis, and Nikolaos Doulamis. 2022. Novel Insights in Spatial Epidemiology Utilizing Explainable AI (XAI) and Remote Sensing. *Remote Sensing* 14, 13 (June 2022), 3074. doi:10.3390/rs14133074
- [65] Getayeneh Antehune Tesema, Zemen Tadesse Tessema, Stephane Heritier, Rob G. Stirling, and Arul Earnest. 2023. A Systematic Review of Joint Spatial and Spatiotemporal Models in Health Research. *International Journal of Environmental Research and Public Health* 20, 7 (March 2023), 5295. doi:10.3390/ijerph20075295
- [66] Ashish Vaswani, Noam Shazeer, Niki Parmar, Jakob Uszkoreit, Llion Jones, Aidan N Gomez, Łukasz Kaiser, and Illia Polosukhin. 2017. Attention is All you Need. (2017).
- [67] Solomon T. Wafula, Oumou Maiga-Ascofare, Nicole S. Struck, Don P. Mathanga, Lauren M. Cohee, Jürgen May, Dewi I. Puradiredja, and Eva Lorenz. 2024. Socioeconomic disparities in Plasmodium falciparum infection risk in Southern Malawi: mediation analyses. *Scientific Reports* 14, 1 (Nov. 2024), 27290. doi:10.1038/s41598-024-78512-1
- [68] Wei Wang, Liu Meng, Zheyu Hu, Xia Yuan, Weisi Zeng, Kunlun Li, Hanjia Luo, Min Tang, Xiao Zhou, Xiaoqiong Tian, Chenhui Luo, Yi He, and Shuo Yang. 2022. The association between outdoor air pollution and lung cancer risk in seven eastern metropolises of China: Trends in 2006–2014 and sex differences. *Frontiers in Oncology* 12 (Sept. 2022). doi:10.3389/fonc.2022.939564 Publisher: Frontiers.
- [69] Elora A. Way, Jenny L. Carwile, Erika C. Ziller, and Katherine A. Ahrens. 2022. Out-of-hospital births and infant mortality in the United States: Effect measure modification by rural maternal residence. *Paediatric and Perinatal Epidemiology* 36, 3 (2022), 399–411. doi:10.1111/ppe.12862 \_eprint: <https://onlinelibrary.wiley.com/doi/pdf/10.1111/ppe.12862>
- [70] Andrea Wendling, Valerie Taglione, Rachel Rezmér, Poe Lwin, Jessica Frost, Julia Terhune, and Jean Kerver. 2021. Access to maternity and prenatal care services in rural Michigan. *Birth* 48, 4 (2021), 566–573. doi:10.1111/birt.12563 \_eprint: <https://onlinelibrary.wiley.com/doi/pdf/10.1111/birt.12563>
- [71] Mathew P. White, Ian Alcock, Benedict W. Wheeler, and Michael H. Depledge. 2013. Would You Be Happier Living in a Greener Urban Area? A Fixed-Effects Analysis of Panel Data. *Psychological Science* 24, 6 (June 2013), 920–928. doi:10.1177/0956797612464659
- [72] World Health Organization (WHO). 2025. *Ill-defined diseases*. Retrieved 2025-01-16 from <https://platform.who.int/mortality/themes/theme-details/MDB/ill-defined-diseases>
- [73] Muhao Xu, Zhenfeng Zhu, Youru Li, Shuai Zheng, Yawei Zhao, Kunlun He, and Yao Zhao. 2024. FlexCare: Leveraging Cross-Task Synergy for Flexible Multimodal Healthcare Prediction. In *Proceedings of the 30th ACM SIGKDD Conference on Knowledge Discovery and Data Mining (KDD '24)*. Association for Computing Machinery, New York, NY, USA, 3610–3620. doi:10.1145/3637528.3671974
- [74] Zhichao Yang, Avijit Mitra, Weisong Liu, Dan Berlowitz, and Hong Yu. 2023. TransformEHR: transformer-based encoder-decoder generative model to enhance prediction of disease outcomes using electronic health records. *Nature Communications* 14, 1 (Nov. 2023), 7857. doi:10.1038/s41467-023-43715-z
- [75] Christopher Yeh, Chenlin Meng, Sherrie Wang, Anne Driscoll, Erik Rozi, Patrick Liu, Jihyeon Lee, Marshall Burke, David B. Lobell, and Stefano Ermon. 2021. SustainBench: Benchmarks for Monitoring the Sustainable Development Goals

- with Machine Learning. <http://arxiv.org/abs/2111.04724> arXiv:2111.04724.
- [76] Ping Yin. 2019. Urban–rural inequalities in spatial accessibility to prenatal care: a GIS analysis of Georgia, USA, 2000–2010. *GeoJournal* 84, 3 (June 2019), 671–683. doi:10.1007/s10708-018-9884-1
- [77] Xueqing Yin, John M. Aiken, Richard Harris, and Jonathan L. Bamber. 2024. A Bayesian spatio-temporal model of COVID-19 spread in England. *Scientific Reports* 14, 1 (May 2024), 10335. doi:10.1038/s41598-024-60964-0 Publisher: Nature Publishing Group.
- [78] Zhihao Yu, Chaohe Zhang, Yasha Wang, Wen Tang, Jiangtao Wang, and Liantao Ma. 2024. Predict and Interpret Health Risk Using Ehr Through Typical Patients. In *ICASSP 2024 - 2024 IEEE International Conference on Acoustics, Speech and Signal Processing (ICASSP)*. 1506–1510. doi:10.1109/ICASSP48485.2024.10447313 ISSN: 2379-190X.
- [79] Chengxi Zang, Yu Hou, Edward J. Schenck, Zhenxing Xu, Yongkang Zhang, Jie Xu, Jiang Bian, Dmitry Morozuk, Dhruv Khullar, Anna S. Nordvig, Elizabeth A. Shenkman, Russell L. Rothman, Jason P. Block, Kristin Lyman, Yiye Zhang, Jay Varma, Mark G. Weiner, Thomas W. Carton, Fei Wang, and Rainu Kaushal. 2024. Identification of risk factors of Long COVID and predictive modeling in the RECOVER EHR cohorts. *Communications Medicine* 4, 1 (July 2024), 130. doi:10.1038/s43856-024-00549-0
- [80] Hanze Zhang, Ningyuan Zhang, Zeyu Li, Jingyuan Yang, Yucheng Zhu, Zhao Liu, and Li Chen. 2024. A higher shadow ratio of the living environment on the remote sensing digital image is possibly protective for adolescent myopia. *Scientific Reports* 14, 1 (Oct. 2024), 23824. doi:10.1038/s41598-024-75486-y
- [81] Hengbiao Zheng, Tao Cheng, Dong Li, Xiang Zhou, Xia Yao, Yongchao Tian, Weixing Cao, and Yan Zhu. 2018. Evaluation of RGB, Color-Infrared and Multispectral Images Acquired from Unmanned Aerial Systems for the Estimation of Nitrogen Accumulation in Rice. *Remote Sensing* 10, 6 (May 2018), 824. doi:10.3390/rs10060824
- [82] Xue-yan Zheng, Si-li Tang, Tao Liu, Ye Wang, Xiao-jun Xu, Ni Xiao, Chuan Li, Yan-jun Xu, Zhao-xuan He, Shu-li Ma, Yu-liang Chen, Rui-lin Meng, and Li-feng Lin. 2022. Effects of long-term PM2.5 exposure on metabolic syndrome among adults and elderly in Guangdong, China. *Environmental Health* 21, 1 (Sept. 2022), 84. doi:10.1186/s12940-022-00888-2

## A Dataset Information

### A.1 Data Scope

We started with data curation in Ohio while participating in the Ohio O-SUDDen program [23]. We noticed the shortage of medical datasets with environmental health risk factors. Therefore, we develop SatHealth, a multimodal public health dataset with environmental factors in multiple categories. We use the data from 2016 to 2022 that is available for all modalities.

We show the scope of SatHealth in Table 7. SatHealth includes monthly aggregated data for climate, air quality, and greenery index at multiple geographical area levels, including counties, ZIP Code Tabulation Areas (ZCTAs), census tracts, and Core Based Statistical Areas (CBSAs). Land cover data in SatHealth is time-independent and denotes the area fraction of multiple land usage types at multiple geographical area levels mentioned above. Moreover, our dataset contains the latest aerial satellite images requested from Google Maps [28]; each image covers a square area around 500m wide. We’ve paid around 2500\$ (including free credits) to extract satellite images from the Google Maps API.

For health-related outcomes, we have the Social Deprivation Index (SDI) in 2019. We also provide yearly prevalences for all diseases identified by ICD codes estimated from medical claims in Ohio extracted from the MarketScan database [45]. We also paid for authorized access to the MarketScan database.

Although SatHealth was created in Ohio using data from 2016–2022, our framework is scalable, and we will gradually cover the whole US and keep updating new data after 2022. We also provide the code for users to create their customer data.

**Table 7: SatHealth Data Scope**

	Spatial Range	Time Span
SatHealth	Ohio	2016-2022
	Spatial Res.	Temporal Res.
Climate/Air Q/Greenery	Cty/ZCTA/CT/CBSA	Month
Land cover	Cty/ZCTA/CT/CBSA	N/A
SDoH (SDI score)	Cty/ZCTA/CT	Year
Disease Prevalence	CBSA	Year
Satellite image	500m×500m per image	N/A

Res.: Resolution; Air Q: Air quality; CBSA: Core Based Statistical Area  
Cty: County; ZCTA: Zip Code Tabulation Area; CT: Census Tract

### A.2 Ethics and Fairness Statement

We list the source and data usage license for components in our dataset in Table 8.

The MarketScan database used in this research is fully Health HIPAA compliant, de-identified, and has very minimal risk of the potential for loss of privacy. We will only publish regional statistics from the original medical claims and exclude regions with fewer than 10 people. Thus, there’s a minimal privacy leakage issue for our medical data.

### A.3 Data License

The dataset is released under the CC BY-SA 4.0 license.

### A.4 Data Access

Users can explore and download our dataset at <https://aimed-sathealth.net> with documentation at <https://github.com/Wang-Yuanlong/SatHealth>. We provide monthly data for climate, air quality, and greenery of multiple cartographic levels mentioned above for users to download. We also offer regional SDI scores and disease prevalence for all ICD codes in the MarketScan database. However, personalized data is not available. Moreover, the collection of satellite images from Google Maps is not available due to copyright concerns, but we provide scripts and a manual for users to extract them from the API Google provided.

## B Dataset Details

### B.1 File Structure

Our dataset and embeddings can be found at <https://aimed-sathealth.net>. We display the downloaded file structure in Table 9.

### B.2 Dataset Components

SatHealth contains multimodal data from multiple sources.

**B.2.1 Environmental Data. ERA5-Land.** ERA5-Land is a global reanalysis dataset developed by the European Centre for Medium-Range Weather Forecasts (ECMWF) under the Copernicus Climate Change Service (C3S). It offers hourly data on land surface variables from 1950 to 5 days before the current date at a resolution of nearly 9km. By focusing on land components, ERA5-Land provides a consistent and detailed depiction of the water and energy cycles over land, making it a valuable resource for hydrological studies,

**Table 8: SatHealth Data Source and License**

Item	Source	Resolution	Frequency	License
Climate/Greenery	ECMWF Climate Reanalysis (ERA5)	11132 m	1 month	link - Terms of Service
Air Q - NO2	Sentinel-5P NRTI NO2	1113.2 m	2 days	link - Data Terms and Conditions
Air Q - Ozone	TOMS and OMI Merged Ozone Data	111000 m	1 day	Data Information Guidance
Air Q - Others	Copernicus Atmosphere Monitoring Service (CAMS)	44528 m	1 day	link - Terms of Service
Greenery - NDVI	Harmonized Sentinel-2 MSI, Level-2A	10 m	5 days	link - Data Terms and Conditions
Land cover	The Copernicus Global Land Service (CGLS)	100 m	1 year	free and open to all users
SDI score	Social Deprivation Index (SDI)	-	-	publicly available
MarketScan CCAE	Merative MarketScan Research Databases	-	-	private
Satellite image	Google Static Map	-	-	link - Terms of Service

Resolution: pixel size when mapped to geographical area; Frequency: time period between records

**Table 9: SatHealth File Structure. Curly bracket ({} ) means there are copies of the same structure for each item in the bracket.**

Raw data		
File	Primary Key	Note
{County, CBSA, ZCTA, CT}/		4 folders for different geo-regions
+ climate.csv	(GEOID, year, month)	
+ greenery.csv	(GEOID, year, month)	
+ airquality.csv	(GEOID, year, month)	
+ landcover.csv	GEOID	
+ sdi.csv	GEOID	Ohio subset of the 2019 SDI downloaded from the SDI website, no CBSA version
+ google_map_points_linked.csv	(GEOID, county, row_idx, col_idx)	Mapping from regions to locations in google_map_points.csv to cover the regions
icd{l1,l2,l3}_prev_ohio.csv	(GEOID, year, code)	
column_dictionary.csv	(table, column)	A collection of column description in all CSV files
google_map_request.py	-	Scripts for requesting satellite images from Google Static Map API given locations
google_map_points.csv	(county, row_idx, col_idx)	A collection of locations used for requesting satellite images
README.md	-	Documentation
Embedding		
File	Primary Key	Note
{County, CBSA, ZCTA, CT}/		4 folders for different geo-regions
+ embedding.csv	(GEOID, year)	
+ embedding_T_agg.csv	(GEOID, year)	Regional environment embeddings enhanced by history embeddings
+ embedding_S_agg.csv	(GEOID, year)	Regional environment embeddings enhanced by neighborhood embeddings
README.md	-	Documentation

numerical weather prediction, and environmental management applications. Our study uses the monthly aggregated version with a subset of variables following [58]. We conduct a regional average reduction of all variables on all cartographic levels we presented before.

**Global Dynamic Land Cover.** The Copernicus Global Land Monitoring Service offers the Global Dynamic Land Cover product, providing annual global land cover maps and cover fraction layers at a 100-meter resolution. These maps are classified into 23 discrete categories based on the UN-FAO Land Cover Classification System, offering detailed insights into Earth’s surface composition. Additionally, the product includes continuous field layers, or "fraction maps," which estimate the proportional coverage of various land cover types within each pixel, enhancing the representation of heterogeneous areas. Our study incorporates the land cover fraction of 9 land cover types following [58]. We conduct a regional average reduction of the cover fractions on all cartographic levels we presented before.

**B.2.2 Satellite Image.** Google Maps and Google Earth use satellite imagery and aerial photography to provide detailed, up-to-date maps. The imagery is sourced from various providers, including high-resolution data from companies like Maxar Technologies (formerly DigitalGlobe), and is processed to create seamless visual representations of Earth’s surface. The Google Maps Static API [28] allows developers to embed these images as static, non-interactive maps into applications via simple HTTP requests, specifying parameters like location, zoom level, size, and markers. This approach offers a lightweight alternative to getting high-quality satellite images without cloud interference at arbitrary locations. We use Google Static Maps API to query images at zoom level 17 to cover Ohio state, which results in 432,918 images. Note that images from Google do not have specific timestamps and may not be well-synchronized. However, this doesn’t matter if we assume the stability of the landscape in several years.

**B.2.3 Social Determinants of Health.** The Social Deprivation Index (SDI), developed by the Robert Graham Center, is a composite measure designed to quantify levels of social disadvantage across small geographic areas in the United States [34]. Utilizing data from the American Community Survey, the SDI incorporates seven demographic characteristics: percentage of individuals in poverty, adults with less than a high school education, single-parent households, rented housing units, overcrowded housing conditions, households without a vehicle, and non-employed adults under 65. SDI converts these census statistics into centiles and combines them to produce the final SDI score. Our dataset includes the county, zip code tabulation area, and census tract-level SDI score in Ohio.

**B.2.4 Health Outcomes.** The IBM MarketScan Commercial Claims and Encounters (CCA) Database is a comprehensive resource that compiles de-identified healthcare claims data from over 250 million individuals in the United States. This database encompasses information from the medical experience of insured employees and their dependents for active employees, early retirees, Consolidated Omnibus Budget Reconciliation Act (COBRA) continues, and Medicare-eligible retirees with employer-provided Medicare Supplemental plans. It integrates detailed records of inpatient and outpatient services, prescription drug claims, and enrollment data, offering a longitudinal perspective on healthcare utilization and expenditures. Our dataset includes 2141777 patients with Ohio residency. We estimated the disease prevalence based on the ICD code occurrence in the dataset.

We create embeddings based on the collected data according to the process described in Section 3. A complete list of variables and image features covered in SatHealth can be found in Table 11.

## C Additional Experimental Details and Results

We put the additional experimental results in this section.

### C.1 Spatiotemporal Generalizability Analysis

In public health studies, a model’s temporal and spatial generalizability is essential as we want our models to be robust as time goes by or when we apply them to other places [65]. Therefore, we conduct additional experiments under spatiotemporal distribution shift cases and provide guidelines for users to develop robust models. All experiments conducted in this section are based on the regional public health modeling task as in Section 4.2.

**C.1.1 Temporal-spatial Generalization Scenarios.** We present three scenarios of spatiotemporal generalization settings: spatial interpolation & extrapolation [27, 57], and temporal forecasting. We simulate the scenarios with SatHealth by designing different cross-validation strategies.

**Spatial interpolation** measures the model ability of within-area prediction [63]. In this setting, regions that are adjacent or close to each other can be dispatched to different folds. Hence, models can leverage similarity between adjacent areas and generalize to adjacent areas. We implement this by randomly splitting regions into K-folds; each fold contains data from all years of its regions.

**Spatial extrapolation** measures the model ability of between-area prediction [63]. In this setting, models are trained in some region clusters and tested in some distant clusters. Therefore, spatial-agnostic patterns captured by the model are evaluated. We implement this by clustering regions by their centroid using K-means and using K clusters as K-folds.

**Temporal forecasting** measures the model’s ability to forecast future outcomes from historical records. This is implemented using the first 4 years (2016-2019) for training and the remaining 3 years (2020-2022) for testing.

**C.1.2 Spatiotemporal Enhanced Regression.** Our dataset can be formalized as  $\mathcal{D} = \{X_r^s, X_{r,t}^d, Y_{r,t}\}_{r \in R, t \in T}$ . Here,  $R$  and  $T$  represent the regions and the timestamps, respectively.  $X_r^s$  denotes static, time-invariant features. For example, we regard satellite images and land cover as static features, as they remain relatively stable over our study period.  $X_{r,t}^d$  denotes time-dependent features, including air quality, climate, and greenery variables.  $Y_{r,t}$  corresponds to health outcomes for each region and year, including SDoH or disease prevalence.

As in Section 4.2, we fit regression models to predict regional SDI and ICD code prevalence by regional environmental representations. We start with the trivial baseline model without any spatiotemporal effect considered. Formally, the baseline regression model can be expressed as:

$$\begin{aligned} Y_{r,t} &= \hat{Y}_{r,t} + \epsilon \\ \hat{Y}_{r,t} &= f(X_r^s, X_{r,t}^d) \end{aligned}$$

$\hat{Y}_{r,t}$  is the estimated outcome,  $f$  is the regression model, and  $\epsilon$  is the unmeasured variation.

Intuitively, regional health outcomes have inherent spatial and temporal autocorrelation because of the similar environment of adjacent regions and gradual temporal shift. Therefore, regression models could benefit from leveraging neighborhood and historical information. Inspired by the boosting strategy for ensemble learning, we introduce the spatiotemporal correlation to the baseline regression model:

$$\begin{aligned} \hat{Y}_{r,t} &= f(X_r^s, X_{r,t}^d) \\ &+ g_s(\{(X_n^s, X_{n,t}^d) \mid n \in N_r\}) + g_t(\{X_{r,h}^d \mid h < t\}) \end{aligned}$$

$X_n^s, X_{n,t}^d$  are environment factors from neighborhood regions  $N_r$  of the region  $r$ ;  $X_{r,h}^d$  are temporal features from history records of the region  $r$ .  $g_s, g_t$  are models learned to account for spatial and temporal information. In our implementation, we consider environmental factors from neighborhoods or history. It will first aggregate the neighborhood and history input features using a weighted sum with an exponential decay factor for history aggregation and constant coefficients for neighborhood aggregation. Then, it fits two regressors for neighborhood and temporal input vectors.

The enhanced model is trained in a boosting manner. We first train  $f$  with the original features and outcomes. Then,  $g_s$  is trained to predict the residual of  $f$ , and  $g_t$  is trained to predict the residual of  $f + g_s$ .

## C.2 Other Experimental Results

Table 10 shows the level-3 ICD codes with the highest prevalence disparity by t-test or odds ratio. It can be seen that the odds ratio results align with Table 3.

We display the feature-disease correlation for top-level and level-3 ICD codes in Figure 5 and 6. The results also show clustering characteristics and similar correlation patterns to Figure 2.

**Table 10: ICD codes with top Urban-rural prevalence disparity by t-test and Odds Ratio**

<b>t-Test</b>				
Category	ICD code	t-statistics	p-value	Description
Urban Prevalent	H02	4.983	0.0003	Other disorders of eyelid
	H00	5.174	0.0005	Hordeolum and chalazion
	L42	4.636	0.0006	Pityriasis rosea
	I78	4.487	0.0007	Diseases of capillaries
	L80	4.353	0.0038	Vitiligo
Rural Prevalent	E16	-6.725	0.0000	Other disorders of pancreatic internal secretion
	K21	-6.469	0.0000	Gastro-esophageal reflux disease
	R01	-5.577	0.0002	Cardiac murmurs and other cardiac sounds
	Z90	-5.290	0.0002	Acquired absence of organs
	N99	-4.962	0.0003	Intraoperative and postprocedural complications and disorders of genitourinary system
<b>Odds Ratio</b>				
Category	ICD code	Odds-ratio	95% CI	Description
Urban Prevalent	P01	4.282	(3.431, 5.343)	Newborn affected by maternal complications of pregnancy
	P03	2.431	(2.115, 2.795)	Newborn affected by other complications of labor and delivery
	P00	2.081	(1.799, 2.407)	Newborn affected by maternal conditions that may be unrelated to present pregnancy
	P54	1.945	(1.358, 2.784)	Other neonatal hemorrhages
	P12	1.863	(1.452, 2.389)	Birth injury to scalp
Rural Prevalent	H68	0.283	(0.237, 0.336)	Eustachian salpingitis and obstruction
	E02	0.371	(0.275, 0.502)	Subclinical iodine-deficiency hypothyroidism
	N42	0.385	(0.330, 0.449)	Other and unspecified disorders of prostate
	D34	0.387	(0.298, 0.503)	Benign neoplasm of thyroid gland
	D13	0.407	(0.354, 0.469)	Benign neoplasm of other and ill-defined parts of digestive system

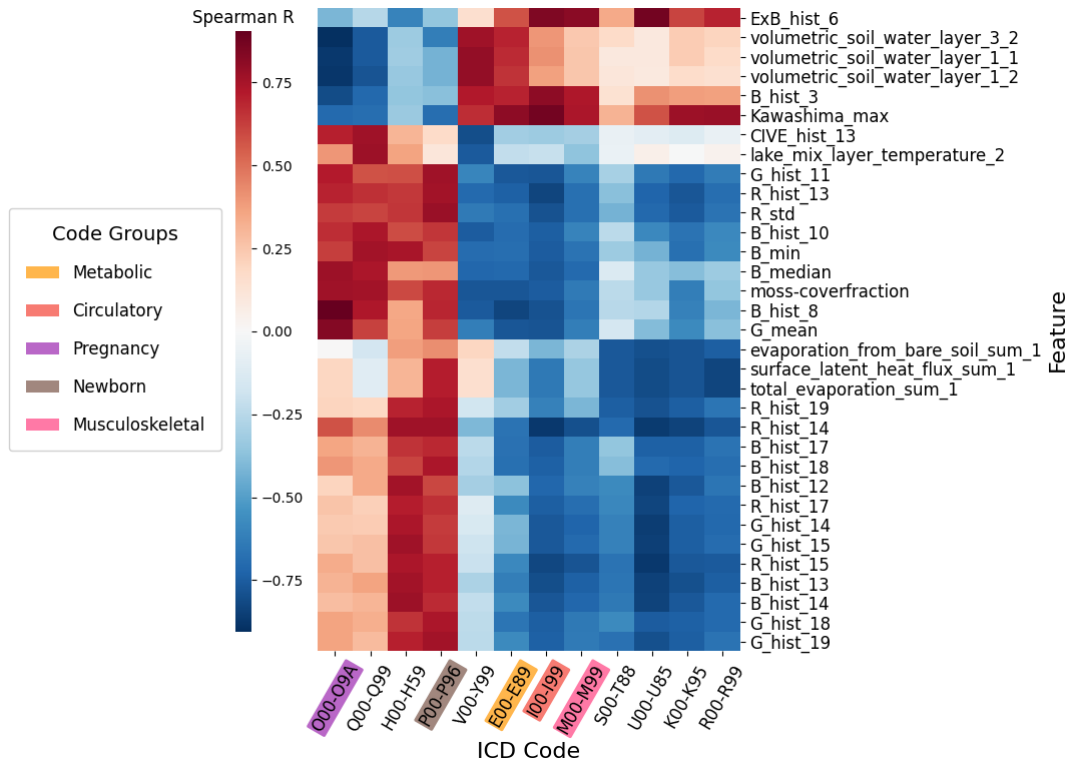


Figure 5: Feature correlations - top level ICD

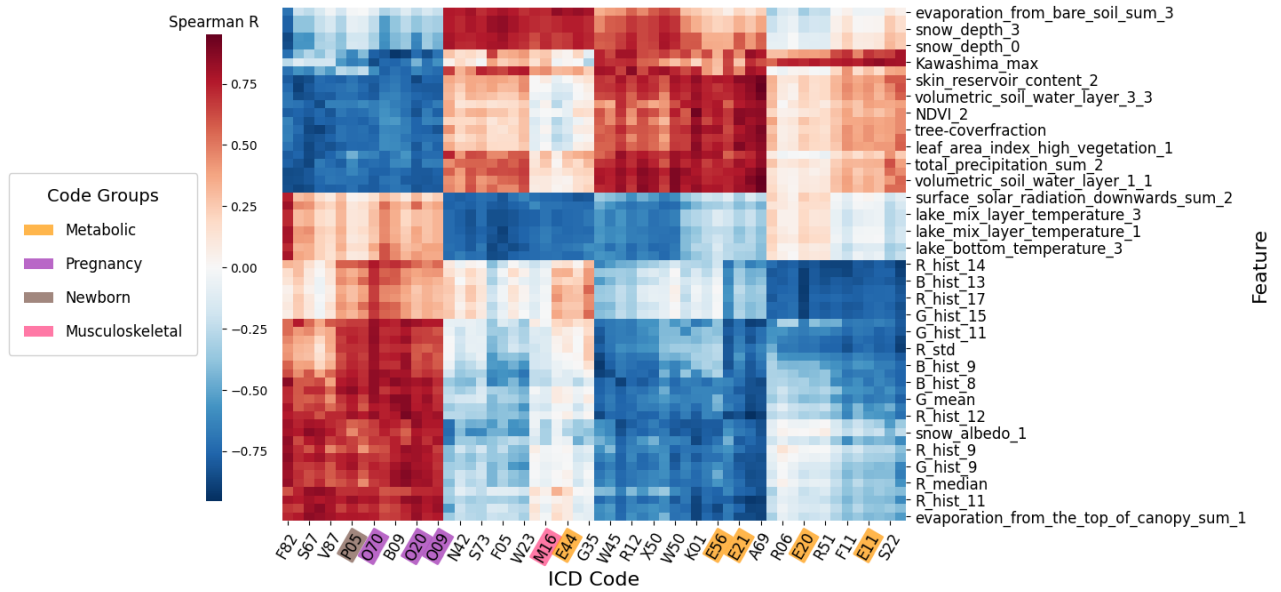


Figure 6: Feature correlations - third level ICD

**Table 11: SatHealth Variables and Features.** Curly bracket (**{}**) means item copies for each item in the bracket.

Category	Variable/Feature	Description
Climate	dewpoint_temperature_2m	Temperature to which the air, at 2 meters above the surface of the Earth, would have to be cooled for saturation to occur.
	temperature_2m	Temperature of air at 2m above the surface of land, sea or in-land waters.
	soil_temperature_level_{1, 3}	Temperature of the soil in different soil layer of the ECMWF Integrated Forecasting System
	lake_bottom_temperature	Temperature of water at the bottom of inland water bodies (lakes, reservoirs, rivers) and coastal waters.
	lake_mix_layer_{depth, temperature}	The thickness/temperature of the upper most layer of an inland water body (lake, reservoirs, and rivers) or coastal waters that is well mixed
	lake_total_layer_temperature	The mean temperature of total water column in inland water bodies (lakes, reservoirs and rivers) and coastal waters.
	snow_albedo, cover, density, depth}	Multiple measurements of snow layer in the ECMWF Integrated Forecast System
	skin_reservoir_content	Amount of water in the vegetation canopy and/or in a thin layer on the soil.
	volumetric_soil_water_layer_{1, 3}	Volume of water in different soil layer of the ECMWF Integrated Forecasting System.
	surface_latent_heat_flux_sum	Exchange of latent heat with the surface through turbulent diffusion.
	surface_net_solar_radiation_sum	Amount of solar radiation reaching the surface of the Earth minus the amount reflected by the Earth's surface.
	surface_solar_thermal_radiation_downwards_sum	Amount of solar radiation (also known as shortwave radiation) reaching the surface of the Earth.
	evaporation_from_bare_soil_sum	Amount of thermal (also known as longwave or terrestrial) radiation emitted by the atmosphere and clouds that reaches the Earth's surface.
	evaporation_from_the_top_of_canopy_sum	The amount of evaporation from the canopy interception reservoir at the top of the canopy.
	evaporation_from_open_water_surfaces_excluding_oceans_sum	Amount of evaporation from surface water storage like lakes and inundated areas but excluding oceans.
	total_evaporation_sum	Accumulated amount of water that has evaporated from the Earth's surface into vapor in the air above.
	{u, v}_component_of_wind_10m	Eastward/Northward component of the 10m wind.
	surface_pressure	Pressure (force per unit area) of the atmosphere on the surface of land, sea and in-land water.
	total_precipitation_sum	Accumulated liquid and frozen water, including rain and snow, that falls to the Earth's surface.
	surface_runoff_sum	Total amount of water accumulated from the beginning of the forecast time to the end of the forecast step
Greenery	leaf_area_index_{high, low}_vegetation	One-half of the total green leaf area per unit horizontal ground surface area for high/low vegetation type.
	NDVI	NDVI index calculated from multispectral image in the area
Air Quality	NDVI_binary	Percentage of pixels with NDVI index above 0.2 in the area
	total_aerosol_optical_depth_at_550nm_surface	Total Aerosol Optical Depth at 550 nm
	particulate_matter_d_less_than_25_um_surface	Concentration of particulate matter $d < 2.5$ $\mu\text{m}$
	NO2_column_number_density	Total vertical column of NO2 (ratio of the slant column density of NO2 and the total air mass factor).
	ozone	Total column ozone
RGB Image Indices	{R,G,B}	Pixel value of Red, Green, and Blue channel. Will use r, g, b for normalized pixel value [ $r=R/(R+G+B)$ , etc.] below.
	Excess Green Index (ExG)	$2 * g - r - b$
	Excess Red Index (ExR)	$1.4 * r - g$
	Excess Blue Index (ExB)	$1.4 * b - g$
	Green Red Vegetation Index (GRVI)	$(G-R)/(G+R)$
	Modified Green Red Vegetation Index (MGRVI)	$(G^2-R^2)/(G^2+R^2)$
	Red Green Blue Vegetation Index (RGBVI)	$(G^2-B^2)/(G^2+B^2)$
Image Embedding Features	Kawashima Index	$(R-B)/(R+B)$
	Color index of vegetation extraction (CIVE)	$0.441r - 0.811g + 0.385b + 18.78745$
	Green leaf index (GLI)	$(2g+r-b)/(2g+r+b)$
		Statistics among all pixels in an image for each index in the above section as <index>
		Number of pixels with index value in histogram bin 0~19 for each index in the above section as <index>